Author Manuscript

Author Manuscript

Author Manuscript

Author Manuscript

HHS Public Access

Author manuscript

Magn Reson Med. Author manuscript; available in PMC 2021 October 20.

Published in final edited form as:

Magn Reson Med. 2021 September ; 86(3): 1420–1433. doi:10.1002/mrm.28815.

3D Whole-Brain Mapping of Cerebral Blood Volume and Venous Cerebral Blood Volume using Fourier-Transform based Velocity-Selective Pulse Trains

Wenbo Li[1,2], **Dapeng Liu**[1,2], **Peter C.M. van Zijl**[1,2], **Qin Qin**[1,2]

[1]The Russell H. Morgan Department of Radiology and Radiological Science, Division of MR Research, Johns Hopkins University School of Medicine, Baltimore, MD, USA

[2]F.M. Kirby Research Center for Functional Brain Imaging, Kennedy Krieger Institute, Baltimore, MD, USA

Abstract

Purpose: To develop 3D MRI methods for cerebral blood volume (CBV) and venous cerebral blood volume (vCBV) estimation with whole-brain coverage using Fourier-transform based velocity-selective (FT-VS) pulse trains.

Methods: For CBV measurement, FT-VS saturation (FT-VSS) pulse trains were employed to suppress static tissue while CSF contamination was corrected voxel-by-voxel using a multi-readout acquisition and a fast CSF T_2 scan. The vCBV mapping was achieved by inserting an arterial-nulling module which included a FT-VS inversion (FT-VSI) pulse train. Using these methods, CBV and vCBV maps were obtained on six healthy volunteers at 3T.

Results: The mean CBV and vCBV values in gray matter and white matter in different areas of the brain showed high correlation ($r = 0.95$ and $p < 0.0001$). The averaged CBV and vCBV values of the whole-brain were 5.4±0.6 and 2.5±0.3 mL/100g in gray matter, and 2.6±0.5 and 1.5±0.2 mL/100g in white matter, respectively, comparable to the literature.

Conclusion: The feasibility of FT-VS based CBV and vCBV estimation was demonstrated for 3D acquisition with large spatial coverage.

Keywords

cerebral blood volume; venous cerebral blood volume; velocity-selective pulse train; arterial nulling; CSF suppression

Introduction

Quantitative estimation of the total cerebral blood volume (CBV) is important to better characterize microvascular physiology in both healthy brains and brain disease. The venous cerebral blood volume (vCBV), which mainly includes the volume of venules, is an important indicator for the venous microvascular homeostasis of the brain[1,2]. The

Corresponding author: Wenbo Li, PhD, F.M. Kirby Research Center for Functional Brain Imaging, Kennedy Krieger Institute, Department of Radiology, Johns Hopkins University School of Medicine, 716 N. Broadway, Baltimore, MD, 21205, wli47@jhmi.edu.

Author Manuscript Author Manuscript Author Manuscript Author Manuscript

increased vCBV could be an indicator of the venous expansion induced by venous congestion[3,4], which could cause leakage of venules and capillaries and in turn lead to brain swelling[5], hyperemia[6,7] or disruption of the blood-brain barrier[8]. Meanwhile, vCBV is critical to further interpret the extravascular BOLD effect[9-11], which results mainly from the change of deoxyhemoglobin concentrations in deoxygenated capillaries, venules and veins. Noninvasive mapping of CBV and vCBV using 3D acquisition with large spatial coverage is desired for both physiological and clinical applications. The main challenge to measure CBV or vCBV is to confine the blood signal to the corresponding vascular compartments[2], which requires suppressing static tissue, mitigating CSF contamination, as well as, for vCBV measurement, nulling arterial, arteriolar and capillary blood.

As an important addition to the technical arsenal of spin tagging MRI, velocity-selective (VS) pulse trains[12] have been developed for direct separation of vascular signal from static tissues. A basic velocity-selective saturation (VSS) pulse train consists of ±90° hard pulses enclosing a pair of adiabatic inversion pulses with surrounding velocity-encoding gradients, which produce a velocity-dependent “cos” modulation. When assuming a laminar flow pattern within the vessels, this VSS module generates a “sinc” modulation, so that the signal of blood flowing above a cutoff velocity (V_{CUTOFF}) gets dephased and the signal of slow moving spins including static tissue is largely preserved. Conventional VSS pulse trains have been employed for measuring cerebral blood flow (CBF)[13,14], venous oxygenation[15-18], arterial CBV[19-21], total CBV[22] and vCBV[23].

Static tissue signal can be subtracted out with VSS modules applied right before acquisition of the interleaved label and control scans[15,16,22,23]. However, the static tissue signal is retained with conventional VSS pulse trains, and system instability and physiological motion could induce fluctuation of the tissue signal. This would generate considerable background error in subtraction, strongly affecting quantification as microvascular signal is only a few percent of static tissue’s signal. A different method applied VS excitation with a “sin” modulation to specifically excite moving spins[17]. This would alleviate the CSF contamination from different diffusion weightings, as well as interference from eddy current effects. However, more than 20% of available blood signal is lost by this scheme[17].

To reduce the CSF contamination of the vascular signal from the pulsatile effect, a CSF suppression module can be applied before the acquisition that nulls residual CSF signal[22]. The scheme of inserting a relatively long T2prep before inversion yields higher vascular signal as a result of saturation recovery compared to using an inversion pulse alone[24]. However, the blood signal is still attenuated due to the limited time available for magnetization recovery of the blood signal. Alternatively, a multi-readout acquisition scheme[25], which takes advantage of large T_2 differences between CSF and blood, can be employed to correct for the CSF partial volume while maintaining high blood signal.

When only the venous signal is targeted, different strategies have been employed for nulling arterial blood. A slab-selective inversion (SSI) under the imaging plane can be applied for nulling the incoming arterial blood[17,18]. However, this method is sensitive to the arterial transit time, which is not ideal for large spatial coverage or patients with occluded vessels. Instead, a conventional VSS module followed by a non-selective inversion (NSI) pulse after

Author Manuscript Author Manuscript Author Manuscript Author Manuscript

a preceding delay can be used to null all recovering arterial blood[15,16]. Another recent study proposed to utilize a single NSI pulse to null fresh incoming arterial blood together with CSF through careful timing[23]. However, this utilization of NSI pulses in the last two schemes also attenuates the available signal of venous blood at acquisition.

As an alternative to the conventional flow-dephasing VSS pulse trains, Fourier-transform based velocity-selective (FT-VS) pulse trains are designed by concatenating a series of small-flip-angle RF pulses followed by paired refocusing pulses with surrounding velocity-encoding gradients[26-28]. These either saturate (FT-VSS) or invert (FT-VSI) static tissue while preserving spins flowing above V_{CUTOFF}. Various FT-VS pulse trains have been applied successfully for MR angiography (MRA)[27,29-34] and quantitative mapping of CBF[26,35] as well as total CBV[28]. FT-VSS label/control modules offer a concurrent capability to suppress the tissue background for more robust CBV measurements[28].

In this work, we aimed to conduct 3D CBV mapping by combining both the FT-VSS pulse train for better tissue suppression[28] and a multi-readout acquisition scheme[25] to remove CSF contamination. Furthermore, we developed a sequence for vCBV quantification by incorporating an arterial blood nulling module which appended the FT-VSI pulse train[26] with an NSI pulse to obtain higher venous blood signal. CBV and vCBV were measured for healthy volunteers with whole-brain coverage at 3T.

Methods

FT-VS Pulse Trains

The FT-VSS and FT-VSI pulse trains[26-28] are composed of nine excitation pulses (10° hard pulses for saturation and 20° hard pulses for inversion), interleaved with paired and phase-cycled refocusing pulses (180° hard pulses) surrounded by gradients with alternating polarity (Figure 1a). The VS label modules (total duration T_{VS} = 96 ms) with triangular gradient lobes (G_{VS} = 29 mT/m; length: 1.2 ms; ramp time: 0.6 ms) yield a targeted saturation or inversion band within ±0.70 cm/s (V_{CUTOFF}, dotted vertical lines in Figures 1b,c). The corresponding control module for FT-VSS also uses velocity-compensated gradient waveforms (dashed lines in Figure 1a) for a more balanced diffusion-weighting effect, and achieves universal saturation regardless of the velocity (dashed horizontal line in Figure 1b). The NSI pulse applied immediately after the FT-VSI pulse train with a spoiling gradient flips the VSI profile such that the flowing spins within the passing band get inverted and the static spins within the inversion band are restored (Figure 1c, red).

Pulse Sequence

The pulse sequence diagrams for CBV and vCBV mapping are shown in Figure 2a. A slab-selective pre-saturation pulse train[36] is used at the start for erasing any magnetization from previous history (yellow square in Figure 2b). For CBV mapping, the FT-VSS label/control modules are applied following a post-saturation delay of 3500 ms. Preceded by fat-suppression, a segmented 3D gradient- and spin-echo (GRASE) readout is used as acquisition. In order to detect the residual CSF signal and correct its contamination in the blood volume analysis, the 208 ms GRASE readout is played out four times after the 90°

Author Manuscript Author Manuscript Author Manuscript Author Manuscript

slab-selective excitation, in which the last readout starting at 624 ms only contain CSF signal and could be used for CSF correction (see Supporting Information Figure S1).

For vCBV mapping, a spatially non-selective arterial-nulling module, which consists of a FT-VSI segment plus an NSI pulse followed by an inversion time (TI), is inserted between the post-saturation delay and the FT-VSS label/control modules. The NSI pulse is a hyperbolic tangent adiabatic pulse (6 ms, maximum amplitude of 13.5 μT, frequency sweep of 12 kHz). The post-saturation delay is set as 2500 ms to allow adequate signal recovery of blood signal after the slab-selective pre-saturation, while letting the fresh incoming arterial blood fill the intracranial arteries in the imaging slab. Figure 3 illustrates the idealized evolution of the microvascular signal through the preparation phase of the sequence. Based on the compartmental microcirculation model[37] previously adopted by other human MRI studies modeling the cerebrovascular network[11,22,38], the velocity ranges in arterioles and venules are [0.4, 4.8] cm/s and [0.2, 2.1] cm/s, while the blood velocity in capillary is as slow as 0.1 cm/s[37]. Therefore, immediately after FT-VSI plus NSI pulses (Figure 3a), the spins flowing above the V_{CUTOFF} (0.7 cm/s) such as those within the arteries, veins and large arterioles and venules would be inverted, while the spins moving below the V_{CUTOFF} such as those within the capillaries and small arterioles and venules, would be preserved (Figure 1c). As shown in Figure 3b and Figure 4a, the inverted blood spins in arteries and large arterioles (velocity > V_{CUTOFF}) would recover and flow into the small arterioles and capillaries, and finally be nulled at the end of TI. Meanwhile, the preserved blood spins in capillaries and small venules (velocity < V_{CUTOFF}) would outflow into the large venules during TI. After the subtraction of the results of FT-VSS control and labeling scans (Figure 3c), only the spins within the venular compartment accelerated above the V_{CUTOFF} will be retained for imaging, and all the spins in capillaries with the flow velocity much slower than V_{CUTOFF} are saturated as shown in Figure 1b.

Considering the T_2 relaxation effect of the relatively long FT-VS pulse trains, Figure 4a shows the simulated magnetization evolution of the blood spins feeding to the arterioles and venules. The T_2 relaxation during the FT-VSI pulses could attenuate the signal both in the inversion band (Figure 4b) and passband (Figure 4c). Therefore, to null the arterial blood, TI is set to be 1050 ms based on the arterial T_1 at 3T of 1.89 s for a Hct of 0.42 [39,40] and an inversion efficiency of FT-VSI+NSI of 0.86 calculated through Bloch equation simulation (more details in Data Analysis). Meanwhile, the capillary blood spins partially attenuated by FT-VSI + NSI pulses will outflow into the venules during TI while recovering to yield relatively high signal for vCBV measurement.

Experiments

All the experiments were conducted on a 3T scanner (Ingenia, Philips Healthcare, Best, The Netherlands) using the body coil for RF transmission (maximum amplitude 13.5 μT) and a 32-channel head coil for signal reception. The maximum strength and slew rate of the gradient coils were 45 mT/m and 200 mT/m/ms, respectively. The protocol was approved by the institutional review board of Johns Hopkins University School of Medicine. All six healthy volunteers (5 females, 1 male, 49+/−12 years old) provided written informed consent.

Author Manuscript Author Manuscript Author Manuscript Author Manuscript

The 3D GRASE readout (Supporting Information Figure S1) was applied with low-high acquisition order. Following the 90° slab-selective excitation pulse, a series of non-selective sinc 180° refocusing pulses were applied. The acquisition parameters were: FOV of 220×220×100 mm^3 with acquisition resolution of 3.5×3.8×5.0 mm^3; slice over sampling factor of 1.6, turbo spin-echo (TSE) factor of 16, echo planar imaging (EPI) factor of 15 along left-right direction, SENSE factor of 2 for phase-encoding, echo spacing of 13 ms and echo train length of 208 ms. The full k-space was acquired with 4 interleaves.

This acquisition scheme was performed for all the following scans. For CBV and vCBV mapping, three additional GRASE readouts were concatenated so that the last readout starting at 624 ms could be used to correct for the remaining CSF signal. These two scans were acquired with a TR of 4.6 s, eight dynamics, and total scan time of 5.5 min. A proton density-weighted image (SI_{PD}) was acquired for CBV/vCBV quantification purposes (TR = 10 s; 1.1 min). Two double inversion recovery (DIR)[41] images were collected to visualize gray matter (TI_1 = 3.58 s; TI_2 = 0.48 s) and white matter (TI_1 = 4.05 s, TI_2 = 0.77 s), respectively (TR = 10 s; 1.1 min).

CSF T_2 was estimated using a method modified from a previous work[42] (Supporting Information Figure S2). The post-saturation delay was set as 9000 ms. A 600 ms T2prep was applied before the acquisition to suppress all other signal except CSF. Eight consecutive GRASE readouts with the same acquisition parameters as the GRASE readout used in vCBV measurement were acquired to obtain the T_2 relaxation decay of CSF signal (TR = 10 s; 1.1 min).

In addition, the arterial-nulling module in the vCBV measurement was incorporated into a VSMRA sequence previously developed[30] to evaluate the arterial nulling effect on one volunteer. Meanwhile, the outflow territories of retained capillary blood during the arterial-nulling module was evaluated using a similar velocity-selective MR angiography (VSMRA) sequence with a modified preparation module, in which the FT-VSI + NSI pulses in the arterial-nulling module were replace by FT-VSI pulse (Supporting Information Figure S5a).

Data analysis:

Matlab (MathWorks, Inc.) was used for data processing. Before analyzing the CBV data, CSF T_2 maps were first derived by fitting the eight datasets voxel-by-voxel as a function of TE using a single exponential decay (Supporting Information Figure S2):

$$S_{CSF} = S_{0,CSF} \times e^{-TE/T_{2,CSF}} \quad [1]$$

This was used to estimate and remove the CSF contamination in the difference images (SI_{diff}) between label and control scans in the CBV measurements at the first and last readouts (ΔTE = 624 ms) using a weighted subtraction (Figure 5):

$$SI_{diff} = SI_{diff,\,first\,readout} - e^{\Delta TE/T_{2,CSF}} \times SI_{diff,\,last\,readout} \quad [2]$$

Author Manuscript Author Manuscript Author Manuscript Author Manuscript

After correcting for the residual CSF signal, the total CBV map was calculated following the process described in our previous paper[28]:

$$CBV = \frac{100 \cdot \lambda \cdot SI_{diff,CBV}}{SI_{PD} \cdot \sum\left(x_i \cdot \alpha_i \cdot M(T_{1,i}) \cdot \left(M(T_{2,i,label}) - M(T_{2,i,control})\right)\right)} \quad [3]$$

in which the unit for CBV is mL blood/100g tissue, and λ is the brain-blood partition coefficient, 0.9 mL of blood/g tissue[43]. SI_{PD} is the signal intensity of the proton density images. For V_{CUTOFF} = 0.70 cm/s, the compartmental fractions of CBV (x_i)[37] and their labeling efficiencies (α_i) are x_a = 0.21, α_a = 0.55 for arterioles and x_v = 0.46, α_v = 0.31 for venules (with negligible contribution from capillary blood: x_c = 0.33; α_c = 0)[28].

The T_1 effects on the blood signals of the three microvascular compartments are determined by the post-saturation recovery:

$$M(T_{1,i}) = 1 - \exp(-T_{recovery} / T_{1,i}) \quad [4]$$

Arterial and venous blood T_1 values were taken[39,40] as $T_{1,a}$ = 1888 ms and $T_{1,v}$ = 1707 ms assuming a Hct of 0.42 and Y_a of 0.98, and Y_v of 0.6 for healthy adults[44,45]. Based on the post-saturation delay of $T_{recovery}$ = 3.5 s in this study, the T_1 effects were calculated as 0.85 for arterial blood and 0.87 for venous blood.

The T_2 effects of blood signal under the label and control modules with duration of T_{VS} can be characterized by[28]:

$$M(T_{2,i,label}) - M(T_{2,i,control}) = k_1 + k_2 \cdot k_3^{k_4 \cdot T_{VS} / T_{2,i}} \quad [5]$$

where [k_1, k_2, k_3, k_4] = [0.12, 0.86, 0.34, 0.38]. Arterial and venous blood T_2 were set as $T_{2,a}$ = 163 ms and $T_{2,v}$ = 71 ms, respectively, based on our T_2 model[39,46] assuming a Hct of 0.42 for the employed 6 ms inter-echo spacing of the FT-VS pulse trains, assuming Hct of 0.42, Y_a of 0.98, and Y_v of 0.6 for healthy adults[44,45]. For the FT-VSS pulse length (T_{VS}) of 96 ms, the T_2 effects were calculated as leading to the normalized magnetization fractions of 0.80 for arterial blood and 0.61 for venous blood.

Regarding the vCBV experiment, the inserted arterial-nulling module (green dashed box in Figure 2a) removes the arterial blood signal. Therefore, vCBV values can be calculated from the CSF corrected signal $SI_{diff,vCBV}$ as

$$vCBV = \frac{100 \cdot \lambda \cdot SI_{diff,vCBV}}{SI_{PD} \cdot \alpha_v \cdot M_{prep} \cdot \left(M(T_{2,v,label}) - M(T_{2,v,control})\right)} \quad [6]$$

where the labeling efficiency α_v (0.31) and the normalized magnetizations after taking into account the T_2 effect during the FT-VSS pulse trains $M(T_{2,v})$ are from Eq. 5. M_{prep} is the magnetization modulation by the post-saturation delay and arterial-nulling module:

$$M_{prep} = 1 + \left(-M(T_{1,c}) \cdot M_{VSI}(T_{2,c}) - 1\right) \cdot e^{-TI / T_1} \quad [7]$$

Author Manuscript Author Manuscript Author Manuscript Author Manuscript

in which $M(T_{1,c})$ represented the normalized blood magnetization after post-saturation recovery (Eq. 4). The negative sign before $M(T_{1,c})$ reflects the inversion by NSI. $M_{VSI}(T_{2,c})$ is the normalized magnetization taking into account the T_2 effect of FT-VSI pulses. As indicated in Figure 3 and 4, the water in the venules at the time of acquisition was originally in the capillary bed when they experienced the FT-VSI pulse train. Therefore, the T_1 and T_2 values of the blood in the capillary will be used to estimate M_{prep}. To estimate T_1 and T_2 values of the blood in the capillary, we used a capillary oxygen delivery model[10] to calculate the blood oxygenation fraction distribution along the capillary and calculated the mean $T_{1,c}$ and $T_{2,c}$ values of the capillary blood as 1861 ms and 118 ms, respectively (Supporting Information S3).

As done in our precious study for the FT-VSS pulse trains[28], this T_2 effect was simulated using the Bloch equation for the FT-VSI pulse train (T_{VS} = 96 ms) with nine different T_2 values of [25, 75, 100, 150, 200, 300, 400, 500] ms, corresponding to sampled T_{VS}/T_2 ratios of [3.84, 1.28, 0.96, 0.64, 0.48, 0.32, 0.24, 0.19]. The averaged magnetizations in the maximal velocity range of [3.5, 7.5] cm/s were calculated as the responses for the FT-VSI module in the passband; the magnetizations for zero velocity were taken as the results of the inversion band (Figure 6a). For convenience of the calculation with different T_2 values, the two datasets were fitted by fitting an empirical 4-parameter model;

$$M_{VSI}(T_2) = a_1 + a_2 \cdot (T_{VS} / T_2) + a_3 \cdot (T_{VS} / T_2)^2 + a_4 \cdot (T_{VS} / T_2)^3 \quad [8]$$

where $[a_1, a_2, a_3, a_4]$ = [0.92, −0.10, 0.0061, 0.0002] for passband (Figure 6b, magenta line) and [−0.97, 0.52, −0.11, 0.011] for inversion band (Figure 6b, green line), respectively.

Therefore, $M(T_{1,c})$, $M_{VSI}(T_{2,c})$ (inversion band for capillary blood), and M_{prep} in Eq. 7 were calculated as 0.74, −0.62 and 0.69, respectively. Meanwhile, using $T_{2,a}$ = 163 ms, the magnetization modulation of FT-VSI on arterial blood (in passband) $M_{VSI}(T_{2,a})$ was calculated as 0.86, which was used to calculate the value of TI for arterial nulling.

Following these equations, the mean CBV and vCBV maps could be obtained from the repeated dynamics. The voxels with large vessels were identified and excluded, through thresholding the CBV map using 12 mL/100g and vCBV map using 6 mL/100g.

For each volunteer, binary gray matter (GM) and white matter (WM) masks were obtained from the GM-only and WM-only DIR images using an empirical threshold. GM and WM ROIs from frontal lobe, temporal lobe, parietal lobe, occipital lobe, and cerebellum were also segmented out. Averaged CBV and vCBV values in GM and WM both from these individual ROIs and the whole brain were calculated.

Results

The CSF correction process is illustrated in Figure 5 using the images acquired with a long effective TE and the separately obtained CSF T_2 map. It can be seen from the figure that the label/control difference image from the first readout still contained a significant portion of CSF signal, likely due to its pulsatile motion, while the label/control difference image from the last readout (ΔTE = 624 ms) only had the remaining CSF signal. Therefore, the

Author Manuscript Author Manuscript Author Manuscript Author Manuscript

CSF contamination in the first readout image was effectively removed by subtracting the label/control difference image of the last readout considering the $T_{2,CSF}$ decay between the first and last readout (Eq. [2]), and the vascular signal was retained as compared with the corresponding DIR GM image. The periventricular gray matter signal (red arrow), which was obscured in the first readout, was represented correctly after the CSF correction.

Axial, coronal, and sagittal planes from 3D whole-brain CBV, vCBV and DIR GM are shown in Figure 7 for two representative subjects. Tissue background was suppressed well and no obvious artifacts related to eddy currents are apparent. When comparing these images, both CBV and vCBV maps have a contrast pattern similar to the DIR GM image due to the high blood volume in the gray matter, and the blood volume values in vCBV maps are roughly half of the values in the CBV maps. Meanwhile, it can be seen that the CSF signals in both CBV and vCBV maps were effectively removed, especially apparent in the ventricular regions. Figure 8 shows five axial CBV and vCBV slices for all six subjects at different locations. The GM/WM contrast of the two maps is largely consistent across subjects.

Figure 9 shows a high correlation ($r = 0.95$ and $p < 0.0001$) between the mean CBV and vCBV values in GM and WM ROIs within the frontal lobe, temporal lobe, parietal lobe, occipital lobe and cerebellum of all our volunteers. The CBV and vCBV values averaged from the whole brain GM and WM tissue masks of each subject are summarized in Table 1. The averaged CBV values in GM and WM are 5.4±0.6 mL/100g and 2.6±0.5 mL/100g, while the averaged vCBV values in GM and WM are 2.5±0.3 mL/100g and 1.5±0.2 mL/100g, respectively.

Discussion

In this work, we optimized a CBV mapping method based on the FT-VSS pulse trains to suppress the static tissue signal and an additional readout with prolonged effective echo time to directly detect CSF contamination. Built on this sequence, a novel technique for quantifying venous CBV was developed by embedding an arterial-nulling module containing a FT-VSI pulse train. The feasibility of both techniques for 3D acquisition with large FOV was demonstrated for a group of healthy volunteers.

Extending from a previous study using 2D acquisition[28], the capability of our new methods is shown in Figures 8 and 9 for 3D CBV quantification with whole-brain coverage. The obtained CBV values (Table 1, averaged 5.4 mL/100g for GM and 2.6 mL/100g for WM) are comparable to those reported previously in the literature[47-51]. The derived vCBV in GM (2.5±0.3 mL/100g) is 46% of the CBV in GM, and comparable to the $x_V = 0.46$ (used in calculating CBV in Eq. [3]) obtained from the above-mentioned compartmental microcirculation model based on animal brain morphological data[37]. For WM, the measured vCBV (1.5±0.2 mL/100g) is about 58% of the CBV, which is a little higher than physiologically plausible, but within error. The inherently low vascular signal in WM inevitably leads to less accuracy and precision for the CBV/vCBV quantification in WM regions compared to GM regions.

Author Manuscript Author Manuscript Author Manuscript Author Manuscript

To detect and then remove the CSF contamination, we adopted a multi-readout strategy previously proposed for a 2D VSASL study[25]. Instead of only acquiring two images with a short TE and a very long TE, our implementation acquired four consecutive images (Figure 2a and Supporting Information Figure S1), with the second and third images not used in the analysis. This consecutive acquisition scheme was chosen in particular for the 3D GRASE readout to keep the echo spacing between the refocusing pulses within each readout the same as the interval between the readouts, and thus alleviate potential artifacts from stimulated echoes.

To estimate the CSF signal attenuation between the first and last readout images, additional CSF T_2 mapping was performed using the same successive GRASE acquisitions (Supporting Information Figure S2). The measured average CSF T_2 for all our volunteers was 2020±231 ms in the ventricles and 1732±288 ms within cortical lobes, which are close to respective values of 2062 ms and 1573 ms reported in a previous study[42] measuring CSF T_2 using separately acquired dataset with different durations of T_2 preparation. Admittedly the CSF T_2 mapping in the current work may have bias induced by B_1 inhomogeneities and a consequent imperfect refocusing of the sinc refocusing pulses used in GRASE readout. However, as the CSF T_2 map sequence shared the same acquisition as the CBV/vCBV sequences, the fitted CSF T_2 values would better reflect the signal decay between the first and last readouts in CBV/vCBV sequences. Instead of employing an extra scan to map CSF T_2, it would be faster and simpler to just apply a single CSF T_2 value for all voxels [25]. If cortical $T_{2,CSF}$ = 1732 ms were presumed, the CSF correction factor, $e^{\Delta TE/T_{2,CSF}}$, would be only overestimated by 5.3% for ventricle $T_{2,CSF}$ = 2020 ms.

To isolate venous blood signal for vCBV quantification, a new arterial-nulling module that combines a FT-VSI pulse train and a NSI pulse (Figure 2a) was applied to preserve the magnetization of the slow flowing blood in capillaries that would flow into the venular vessels during TI (Figures 3 and 4). The Supporting Information Figure S4 shows that, in this limited dataset, velocity-selective MR angiography (VSMRA) employing this arterial-nulling module confirms its effectiveness to suppress the signal in distal arteries to a level of less than 10%. This ensured a very minimal vCBV signal contribution from small arteries and arterioles, because the arterial blood bolus containing inverted spins (Figure 3a) would flow downstream and fill both small arteries and arterioles during TI and finally get nulled at the time of acquisition as illustrated in Figure 3b. Notably, as shown in Supporting Information Figure S4a, some signal remains in large arteries such as middle cerebral arteries due to the fast inflow of fresh arterial blood during TI. However, these large vessels, which could not be fully suppressed by the arterial-nulling module, would be removed through thresholding as described in Data Analysis and thus have little impact on vCBV measurement. Another possible limitation of the arterial-nulling module is that imperfect inversion by the FT-VSI plus NSI pulses caused for instance by B_1 inhomogeneity could induce a residual arterial signal. If the inversion efficiency were 0.66, 23% lower than 0.86 used above, an 11% arterial signal will be left after the TI. Considering the arterial blood volume fraction is less than half of the venous blood volume fraction (0.21 vs 0.46 based on the compartmental microcirculation model[37]), this remaining 11% arterial signal would induce only around 5% overestimation of vCBV.

Author Manuscript Author Manuscript Author Manuscript Author Manuscript

In addition, in the arterial-nulling module for our vCBV estimation, we also assumed that the capillary blood retained by the FT-VSI and NSI pulses will move out and fill the venules and small veins during the TI as depicted in Figure 3. To visualize the correctness of this assumption regarding the outflow territory of the capillary blood during TI, we designed a VSMRA sequence with a modified preparation module, in which the FT-VSI + NSI pulses in the arterial-nulling module were replace by FT-VSI pulse (Supporting Information Figure S5a). In this sequence, the FT-VSI pulse will invert the capillary blood below the V_{CUTOFF} (Figure 1c, black line) and the inverted capillary blood will flow out into the venules and cortical veins during TI and be nulled at acquisition (Supporting Information Figure S5b). Then the outflow territories of the capillary blood can be illustrated by comparing the VSMRA with and without this modified preparation module. As shown in Supporting Information Figure S5c, most of the visible cortical veins were nulled, which indicates that the outflowing capillary blood reached these large cortical veins during TI. This suggest that our vCBV estimation targeting on the venules and small veins may not be very susceptible to variations in venous flow velocity, which would require further validation over a larger population. Of course for reduced flow situations, such as in the presence of the venous congestion, our method could underestimate vCBV values.

In the quantitative CBV/vCBV maps (Eq. [3-8]), the signal evolution during the post-saturation delay or the following arterial-nulling module and FT-VSS module is estimated based on the T_1 and T_2 values of arterial and venous blood calculated from the population-averaged Hct (0.42) and Y_v (0.60) values[44,45]. To evaluate the sensitivity of the CBV/vCBV measurements to Hct and Y_v variations, Hct and Y_v were sampled from the range [0.39, 0.50] with interval of 0.005 and [0.50, 0.70] with interval of 0.01, respectively. For a given combination of Hct and Y_v, the blood T_1 and T_2 values were derived based on our published models[39,40,46]. The corresponding CBV/vCBV results were compared with the ones obtained using Hct of 0.42 and Yv of 0.60. As shown in Supporting Information Figure S6, the variation of Hct in the range of [0.39, 0.50] and Yv in the range of [0.50, 0.70] could cause deviations of up to [−6%, 9%] and [−15%, 24%] in the CBV and vCBV estimations, respectively. To minimize these potential biases, individual measurements of arterial blood T_1 and venous blood T_2 values could be measured with each taking around 1 min respectively[45,52-57]. These can be used to calculate Hct and Yv, respectively using an available on-line calculator[39]. Meanwhile, in the vCBV estimation, T_1 and T_2 values of capillary blood (1861 ms and 118 ms) were used to calculate the magnetization modulation imposed by the post-saturation delay and arterial-nulling module. However, due to the fast water exchange between the capillary bed and tissue, the relaxation of tissue water would also affect the venous signal. If the T_1 and T_2 values of GM (T_1 = 1165ms and T_2 = 83 ms) and WM (T_1 = 738 ms and T_2 = 75 ms)[58] were used, there would be a 11% and 20% difference in the estimated vCBV values, respectively.

Furthermore, to calculate the labeling efficiency α_i in Eqs. [3] and [6], the volume fractions of arterial, venous and capillary blood and their corresponding velocities[28] were also assumed based on a compartmental microcirculation model[37]. However, this assumption may not be valid under conditions such as brain pathologies, CVR challenges, or functional stimulation. Given these considerations, we calculated the labeling efficiency α_i in Eq. [3] and [6], and found that a 20% change in blood velocity could lead to 8% deviation in

Author Manuscript Author Manuscript Author Manuscript Author Manuscript

the arterial labeling efficiency α_a and 14% deviation in the venous labeling efficiency α_v. Meanwhile, the arterial and venous compartmental fractions (x_i in Eq. [3]) would change under hypercapnia and visual stimulation challenges due to the different vascular response among arterioles, capillaries and venules/veins. Previous studies[59,60] have shown that vCBV change would contribute about 36%-50% of total CBV change under hypercapnia and visual stimulation. Based on these results and the assumption that the capillary has little change during the stimulation[61,62], there would be a 10%~13% overestimation of our CBV measurement if the total CBV increases 20% under certain stimulation. Certainly, if brain capillary also involves in CBF regulation and dilates under stimulations as indicated by recent study[63], the overestimation of our CBV measurement will decrease due to the less change of x_i values. Note that our vCBV computation (Eq. [6]) does not depend on venous compartment fraction x_v and thus would not be affected by its change in the stimulation.

The T_2 effect during the FT-VSS and FT-VSI pulse trains can in principle be lowered by shortening their duration (T_{VS}), e.g. when having availability of higher maximum B_1 amplitude and a higher maximum amplitude and slew rate for the gradient system. If T_{VS} were reduced from 96 ms to 64 ms, the normalized magnetization difference $M(T_{2,i,label})$-$M(T_{2,i,control})$ (Eq. [5]) would be raised from 0.79 to 0.85 for arterial blood ($T_{2,a}$ = 163 ms) and from 0.61 to 0.71 for venous blood ($T_{2,v}$ = 71 ms); $M_{VSI}(T_2)$ (Eq. [8]) for the capillary blood ($T_{2,c}$ = 118 ms) would be improved from −0.62 to −0.72 and M_{prep} would be improved from 0.69 to 0.74.

Note that the duration of each GRASE readout was relatively long (T_{acq} = 208 ms) compared to venous blood T_2 ($T_{2,v}$ = 71 ms). Optimum T_{acq} /T_2 ratio to mitigate T_2-decay induced blurring and achieve maximum SNR efficiency is 1.2 [64]. Thus a T_{acq} of 100 ms would be more desirable, especially for vCBV mapping. More advanced acceleration techniques could further improve the temporal resolution of the acquisition.

Conclusion

We extended the FT-VSS based CBV mapping technique from 2D to 3D acquisition with suppression of static tissue and mitigation of CSF contamination. We further demonstrated a vCBV quantification method with preservation of high venular signal by applying a FT-VSI pulse train. The clinical value of these approaches is expected to be especially for patients with cerebrovascular disease, where blood transit times are unknown. In addition, the ability to determine vCBV should be helpful for the quantitative interpretation of BOLD effects.

Supplementary Material

Refer to Web version on PubMed Central for supplementary material.

Acknowledgment

We thank Joseph Gillen, Terri Brawner, Ivana Kusevic and Kathleen Kahl for their experimental assistance. Dr. van Zijl is a paid lecturer for Philips Healthcare, has research support from Philips, and has technology licensed to Philips. This has been approved by the Committee on Conflict of Interest of Johns Hopkins University.

Author Manuscript Author Manuscript Author Manuscript Author Manuscript

Grant support:

NIH: P41 EB015909 (PvZ); NIH: P41 EB031771(PvZ); NIH: K25 HL145129 (WL); NIH S10 OD021648; NIH: R01 HL138182 (QQ), NIH: R01 HL144751 (QQ); Scholar Award of American Society of Hematology (QQ).

Reference

1. Schaller B Physiology of cerebral venous blood flow: from experimental data in animals to normal function in humans. Brain Res Rev. 2004;46(3):243–260. [PubMed: 15571768]
2. Hua J, Liu P, Kim T, et al. MRI techniques to measure arterial and venous cerebral blood volume. Neuroimage. 2019;187(2 2018):17–31. [PubMed: 29458187]
3. Houck AL, Gutierrez J, Gao F, et al. Increased diameters of the internal cerebral veins and the basal veins of Rosenthal are associated with white matter hyperintensity volume. Am J Neuroradiol. 2019;40(10):1712–1718. [PubMed: 31515212]
4. Lou M, Zhang J, Wang Y, et al. Cerebral Venous System in Acute and Chronic Brain Injuries.; 2019.
5. Yu W, Rives J, Welch B, White J, Stehel E, Samson D. Hypoplasia or occlusion of the ipsilateral cranial venous drainage is associated with early fatal edema of middle cerebral artery infarction. Stroke. 2009;40(12):3736–3739. [PubMed: 19762692]
6. Nakase H, Heimann A, Kempski O. Local cerebral blood flow in a rat cortical vein occlusion model. J Cereb Blood Flow Metab. 1996;16(4):720–728. [PubMed: 8964813]
7. Al-Rodhan NRF, Sundt TM, Piepgras DG, Nichols DA, Rufenacht D, Stevens LN. Occlusive hyperemia: A theory for the hemodynamic complications following resection of intracerebral arteriovenous malformations. J Neurosurg. 1993;78(2):167–175. [PubMed: 8421198]
8. Mayhan WG, Heistad DD. Role of veins and cerebral venous pressure in disruption of the blood-brain barrier. Circ Res. 1986;59(2):216–220. [PubMed: 3742745]
9. Ogawa S, Menon RS, Tank DW, et al. Functional brain mapping by blood oxygenation level-dependent contrast magnetic resonance imaging. A comparison of signal characteristics with a biophysical model. Biophys J. 1993;64(3):803–812. [PubMed: 8386018]
10. Buxton RB, Frank LR. A model for the coupling between cerebral blood flow and oxygen metabolism during neural stimulation. J Cereb Blood Flow Metab. 1997;17(1):64–72. [PubMed: 8978388]
11. Van Zijl PCM, Eleff SM, Ulatowski JA, et al. Quantitative assessment of blood flow, blood volume and blood oxygenation effects in functional magnetic resonance imaging. Nat Med. 1998;4:159–167. [PubMed: 9461188]
12. Norris DG, Schwarzbauer C. Velocity Selective Radiofrequency Pulse Trains. J Magn Reson. 1999;137(1):231–236. [PubMed: 10053152]
13. Wong EC, Cronin M, Wu W-C, Inglis B, Frank LR, Liu TT. Velocity-selective arterial spin labeling. Magn Reson Med. 2006;55(6):1334–1341. [PubMed: 16700025]
14. Duhamel G, De Bazelaire C, Alsop DC. Evaluation of systematic quantification errors in velocity-selective arterial spin labeling of the brain. Magn Reson Med. 2003;50(1):145–153. [PubMed: 12815689]
15. Bolar DS, Rosen BR, Sorensen AG, Adalsteinsson E. QUantitative Imaging of eXtraction of oxygen and TIssue consumption (QUIXOTIC) using venular-targeted velocity-selective spin labeling. Magn Reson Med. 2011;66(6):1550–1562. [PubMed: 21674615]
16. Stout JN, Adalsteinsson E, Rosen BR, Bolar DS. Functional oxygen extraction fraction (OEF) imaging with turbo gradient spin echo QUIXOTIC (Turbo QUIXOTIC). Magn Reson Med. 2018;79(5):2713–2723. [PubMed: 28984056]
17. Guo J, Wong EC. Venous oxygenation mapping using velocity-selective excitation and arterial nulling. Magn Reson Med. 2012;68(5):1458–1471. [PubMed: 22294414]
18. Liu EY, Guo J, Simon AB, Haist F, Dubowitz DJ, Buxton RB. The potential for gas-free measurements of absolute oxygen metabolism during both baseline and activation states in the human brain. Neuroimage. 2020;207:116342. [PubMed: 31722231]
19. Petersen ET, Lim T, Golay X. Model-free arterial spin labeling quantification approach for perfusion MRI. Magn Reson Med. 2006;55(2):219–232. [PubMed: 16416430]

Author Manuscript Author Manuscript Author Manuscript Author Manuscript

20. Van Westen D, Petersen ET, Wirestam R, et al. Correlation between arterial blood volume obtained by arterial spin labelling and cerebral blood volume in intracranial tumours. Magn Reson Mater Physics, Biol Med. 2011;24(4):211–223.
21. Hua J, Qin Q, Pekar JJ, van Zijl PCM. Measurement of absolute arterial cerebral blood volume in human brain without using a contrast agent. NMR Biomed. 2011;24(10):1313–1325. [PubMed: 21608057]
22. Liu D, Xu F, Lin DD, van Zijl PCM, Qin Q. Quantitative measurement of cerebral blood volume using velocity-selective pulse trains. Magn Reson Med. 2017;77(1):92–101. [PubMed: 27797101]
23. Lee H, Wehrli FW. Venous cerebral blood volume mapping in the whole brain using venous-spin-labeled 3D turbo spin echo. Magn Reson Med. 2020;Epub ahead.
24. Wong EC, Liu TT, Luh W-M, Frank LR, Buxton RB. T1 andT2 selective method for improved SNR in CSF-attenuated imaging:T2-FLAIR. Magn Reson Med. 2001;45(3):529–532. [PubMed: 11241715]
25. Guo J, Wong EC. Removal of CSF contamination in VSASL and QUIXOTIC using a long TE CSF Scan. Proc 19th Annu Meet ISMRM. 2011:2116.
26. Qin Q, van Zijl PCM. Velocity-selective-inversion prepared arterial spin labeling. Magn Reson Med. 2016;76(4):1136–1148. [PubMed: 26507471]
27. Qin Q, Shin T, Schär M, Guo H, Chen H, Qiao Y. Velocity-selective magnetization-prepared non-contrast-enhanced cerebral MR angiography at 3 Tesla: Improved immunity to B0/B1 inhomogeneity. Magn Reson Med. 2016;75(3):1232–1241. [PubMed: 25940706]
28. Qin Q, Qu Y, Li W, et al. Cerebral blood volume mapping using Fourier-transform–based velocity-selective saturation pulse trains. Magn Reson Med. 2019;81:3544. [PubMed: 30737847]
29. Shin T, Worters PW, Hu BS, Nishimura DG. Non-contrast-enhanced renal and abdominal MR angiography using velocity-selective inversion preparation. Magn Reson Med. 2013;69(5):1268–1275. [PubMed: 22711643]
30. Li W, Xu F, Schär M, et al. Whole-brain arteriography and venography: Using improved velocity-selective saturation pulse trains. Magn Reson Med. 2018;79(4):2014. [PubMed: 28799210]
31. Zhu D, Li W, Liu D, et al. Non-contrast-enhanced abdominal MRA at 3 T using velocity-selective pulse trains. Magn Reson Med. 2020;84(3):173.
32. Shin T, Hu BS, Nishimura DG. Off-resonance-robust velocity-selective magnetization preparation for non-contrast-enhanced peripheral MR angiography. Magn Reson Med. 2013;70(5):1229–1240. [PubMed: 23192893]
33. Shin T, Qin Q. Characterization and suppression of stripe artifact in velocity-selective magnetization-prepared unenhanced MR angiography. Magn Reson Med. 2018;80(5):1997–2005. [PubMed: 29536569]
34. Shin T, Qin Q, Park JY, Crawford RS, Rajagopalan S. Identification and reduction of image artifacts in non–contrast-enhanced velocity-selective peripheral angiography at 3T. Magn Reson Med. 2016;76(2):466–477. [PubMed: 26308243]
35. Liu D, Xu F, Li W, Van Zijl PCM, Lin DD, Qin Q. Improved velocity-selective-inversion arterial spin labeling for cerebral blood flow mapping with 3D acquisition. Magn Reson Med. 2020;84(5):2512–2522. [PubMed: 32406137]
36. Ogg RJ, Kingsley PB, Taylor JS. WET, a T1- and B1-insensitive water-suppression method for in vivo localized 1H NMR spectroscopy. J Magn Reson Ser B. 1994;104(1):1–10. [PubMed: 8025810]
37. Sharan M, Jones MD, Koehler RC, Traystman RJ, Popel AS. A compartmental model for oxygen transport in brain microcirculation. Ann Biomed Eng. 1989;17(1):13–38. [PubMed: 2919811]
38. Piechnik SK, Chiarelli PA, Jezzard P. Modelling vascular reactivity to investigate the basis of the relationship between cerebral blood volume and flow under CO2 manipulation. Neuroimage. 2008;39(1):107–118. [PubMed: 17920935]
39. Li W, van Zijl PCM. Blood T2, T1 calculator. http://godzilla.kennedykrieger.org/cgi-bin/bloodT2T1_cal.pl.
40. Li W, Grgac K, Huang A, Yadav N, Qin Q, Van Zijl PCM. Quantitative theory for the longitudinal relaxation time of blood water. Magn Reson Med. 2016;76(1):270–281. [PubMed: 26285144]

Author Manuscript Author Manuscript Author Manuscript Author Manuscript

41. Redpath TW, Smith FW. Technical note: Use of a double inversion recovery pulse sequence to image selectively grey or white brain matter. Br J Radiol. 1994;67(804):1258–1263. [PubMed: 7874427]
42. Qin Q A simple approach for three-dimensional mapping of baseline cerebrospinal fluid volume fraction. Magn Reson Med. 2011;65(2):385–391. [PubMed: 21264932]
43. Herscovitch P, Raichle ME. What is the correct value for the brain--blood partition coefficient for water? J Cereb Blood Flow Metab. 1985;5(1):65–69. [PubMed: 3871783]
44. Lu H, Xu F, Grgac K, Liu P, Qin Q, van Zijl PCM. Calibration and validation of TRUST MRI for the estimation of cerebral blood oxygenation. Magn Reson Med. 2012;67(1):42–49. [PubMed: 21590721]
45. Qin Q, Grgac K, van Zijl PCM. Determination of whole-brain oxygen extraction fractions by fast measurement of blood T(2) in the jugular vein. Magn Reson Med. 2011;65(2):471–479. [PubMed: 21264936]
46. Li W, van Zijl PCM. Quantitative theory for the transverse relaxation time of blood water. NMR Biomed. 2020;33:4207.
47. Sakai F, Nakazawa K, Tazaki Y, et al. Regional cerebral blood volume and hematocrit measured in normal human volunteers by single-photon emission computed tomography. J Cereb Blood Flow Metab. 1985;5(2):207–213. [PubMed: 3921557]
48. Leenders KLKL, Perani D, Lammertsma AA, et al. Cerebral blood flow, blood volume and oxygen utilization: Normal values and effect of age. Brain. 1990;113(1):27–47. [PubMed: 2302536]
49. Uh J, Lewis-Amezcua K, Varghese R, Lu H. On the measurement of absolute cerebral blood volume (CBV) using vascular-space-occupancy (VASO) MRI. Magn Reson Med. 2009;61(3):659–667. [PubMed: 19097238]
50. Bjørnerud A, Emblem KE. A fully automated method for quantitative cerebral hemodynamic analysis using DSC-MRI. J Cereb Blood Flow Metab. 2010;30(5):1066–1078. [PubMed: 20087370]
51. Knutsson L, Lindgren E, Ahlgren A, et al. Dynamic susceptibility contrast MRI with a prebolus contrast agent administration design for improved absolute quantification of perfusion. Magn Reson Med. 2014;72(4):996–1006. [PubMed: 24285621]
52. Qin Q, Strouse JJ, van Zijl PCM. Fast measurement of blood T1 in the human jugular vein at 3 Tesla. Magn Reson Med. 2011;65(5):1297–1304. [PubMed: 21500258]
53. Li W, Liu P, Lu H, Strouse JJ, van Zijl PCM, Qin Q. Fast measurement of blood T1 in the human carotid artery at 3T: Accuracy, precision, and reproducibility. Magn Reson Med. 2017;77:2296. [PubMed: 27436420]
54. Lu H, Ge Y. Quantitative evaluation of oxygenation in venous vessels using T2-Relaxation-Under-Spin-Tagging MRI. Magn Reson Med. 2008;60(2):357–363. [PubMed: 18666116]
55. Varela M, Hajnal J V, Petersen ET, Golay X, Merchant N, Larkman DJ. A method for rapid in vivo measurement of blood T1. NMR Biomed. 2011;24(1):80–88. [PubMed: 20669148]
56. Wu WC, Jain V, Li C, et al. In vivo venous blood T1 measurement using inversion recovery true-FISP in children and adults. Magn Reson Med. 2010;64(4):1140–1147. [PubMed: 20564586]
57. Zhang X, Petersen ET, Ghariq E, et al. In vivo blood T1 measurements at 1.5 T, 3 T, and 7 T. Magn Reson Med. 2013;70:1082–1086. [PubMed: 23172845]
58. Lu H, Nagae-Poetscher LM, Golay X, Lin D, Pomper M, Van Zijl PCM. Routine clinical brain MRI sequences for use at 3.0 tesla. J Magn Reson Imaging. 2005;22(1):13–22. [PubMed: 15971174]
59. Kim T, Kim SG. Temporal dynamics and spatial specificity of arterial and venous blood volume changes during visual stimulation: Implication for BOLD quantification. J Cereb Blood Flow Metab. 2011;31(5):1211–1222. [PubMed: 21179068]
60. Lee SP, Duong TQ, Yang G, Iadecola C, Kim SG. Relative changes of cerebral arterial and venous blood volumes during increased cerebral blood flow: Implications for bold fMRI. Magn Reson Med. 2001;45(5):791–800. [PubMed: 11323805]
61. Hill RA, Tong L, Yuan P, Murikinati S, Gupta S, Grutzendler J. Regional Blood Flow in the Normal and Ischemic Brain Is Controlled by Arteriolar Smooth Muscle Cell Contractility and Not by Capillary Pericytes. Neuron. 2015;87(1):95–110. [PubMed: 26119027]

Author Manuscript Author Manuscript Author Manuscript Author Manuscript

62. Fernández-Klett F, Offenhauser N, Dirnagl U, Priller J, Lindauer U. Pericytes in capillaries are contractile in vivo, but arterioles mediate functional hyperemia in the mouse brain. Proc Natl Acad Sci U S A. 2010;107(51):22290–22295. [PubMed: 21135230]

63. Cai C, Fordsmann JC, Jensen SH, et al. Stimulation-induced increases in cerebral blood flow and local capillary vasoconstriction depend on conducted vascular responses. Proc Natl Acad Sci U S A. 2018;115(25):E5796–E5804. [PubMed: 29866853]

64. Qin Q Point spread functions of the T2 decay in k-space trajectories with long echo train. Magn Reson Imaging. 2012;30(8):1134–1142. [PubMed: 22817958]

Author Manuscript Author Manuscript Author Manuscript Author Manuscript

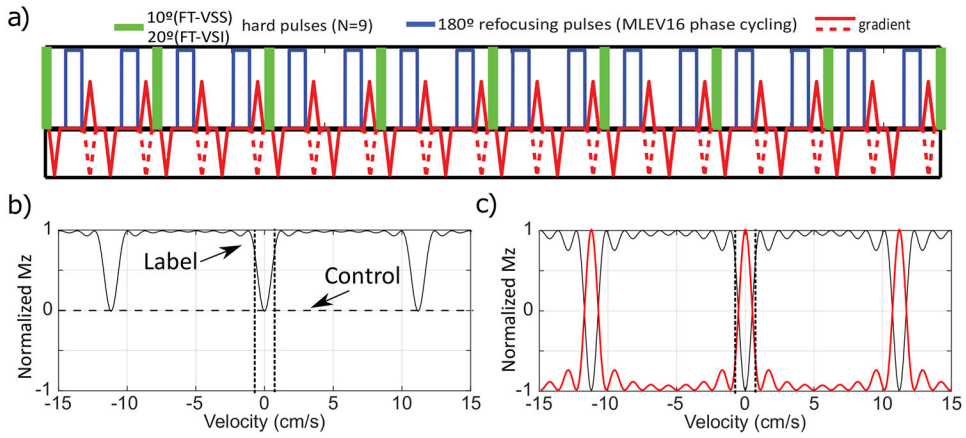

Figure 1.

a) Diagram of Fourier-Transform based velocity-selective saturation (FT-VSS) and inversion (FT-VSI) pulse trains. b) Mz-velocity response for FT-VSS. The horizontal dashed line illustrates the universal saturation response of the control module. The V_{CUTOFF}s at ±0.7 cm/s are indicated by the vertical dotted lines. c) Mz-velocity response for FT-VSI alone (black) and the flipped one after a following non-selective inversion (NSI) pulse (red).

Author Manuscript Author Manuscript Author Manuscript Author Manuscript

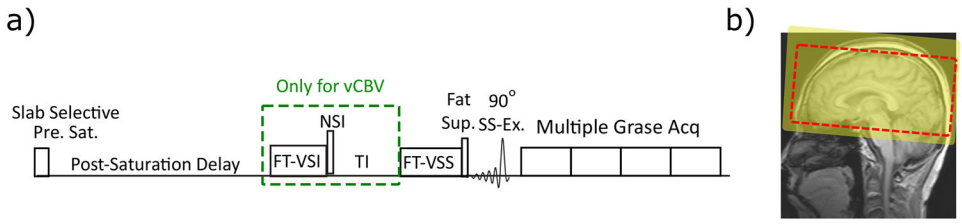

Figure 2.

a) General outline of the pulse sequences for CBV and vCBV measurement. Both include slab-selective pre-saturation, FT-VSS label/control pulse trains, fat-suppression, and 3D GRASE readout with multiple repetitions. For vCBV quantification, a spatially non-selective arterial-nulling module is added after the post-saturation delay (the green dashed box). b) The location of the imaging FOV (dashed red box) and the pre-saturation (yellow-shaded rectangular area).

Author Manuscript Author Manuscript Author Manuscript Author Manuscript

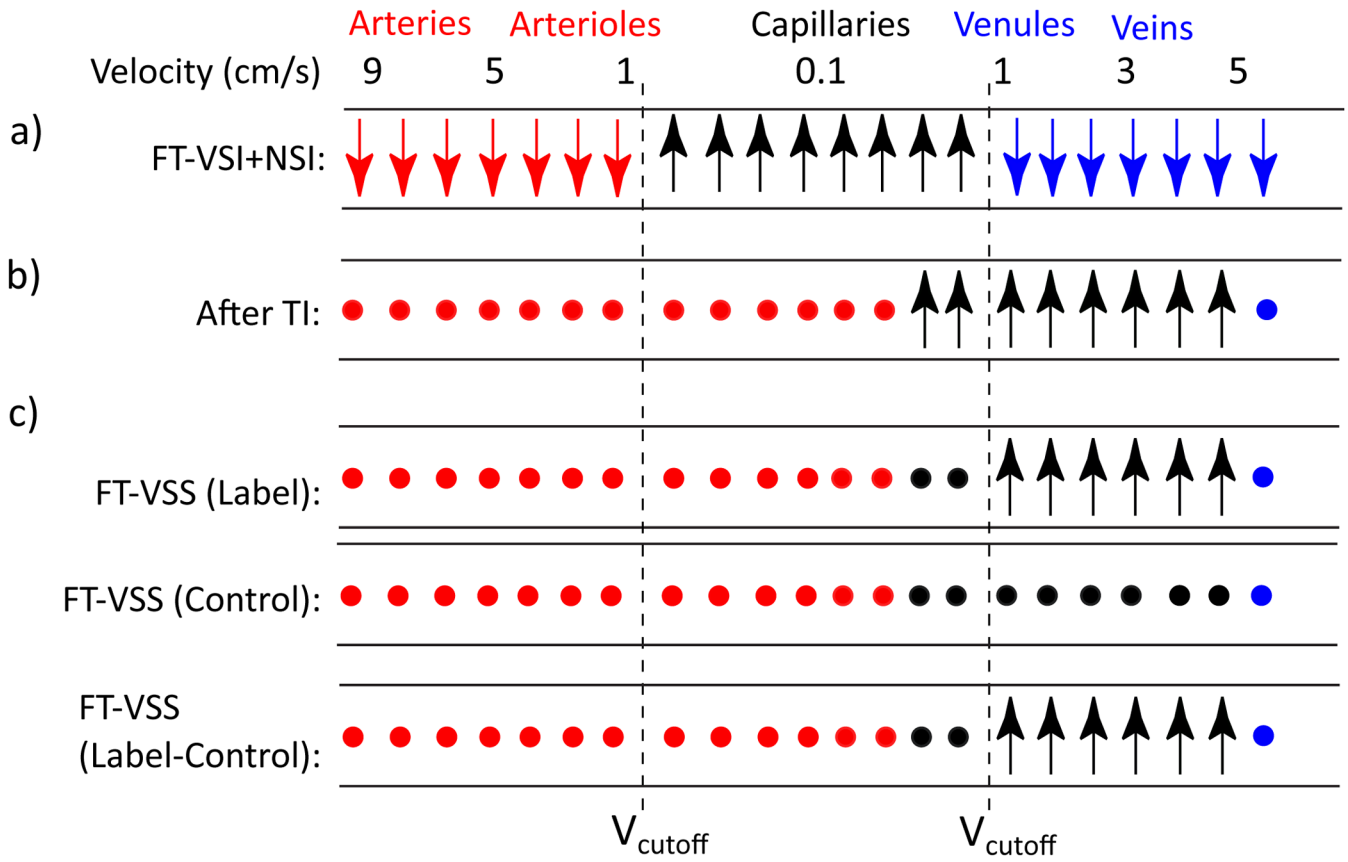

Figure 3.

Idealized cartoon depicting the evolution of the longitudinal magnetization of water in different compartments with the goal of venular signal isolation. Preserved, inverted and nulled spins are denoted by upright arrows, downright arrows and solid circles, respectively. The consecutive FT-VSI and NSI pulses invert spins in arteries/large arterioles (red) and large venules/veins (blue) flowing above the V_{CUTOFF} and preserve the spins in capillaries as well as small arterioles and veins (black) moving below the V_{CUTOFF}. The inverted arterial (red) and venous (blue) blood are nulled at TI and the downstream arterial blood will flow into capillaries. Meanwhile, the spins with preserved magnetization (in black) will flow out from the capillary bed into the venules during the inversion time (TI). The final FT-VSS label/control modules separate out the venular signal before data acquisition. FT-VSS or FT-VSI: Fourier-Transform based velocity-selective saturation or inversion. NSI: Non-selective inversion.

Author Manuscript Author Manuscript Author Manuscript Author Manuscript

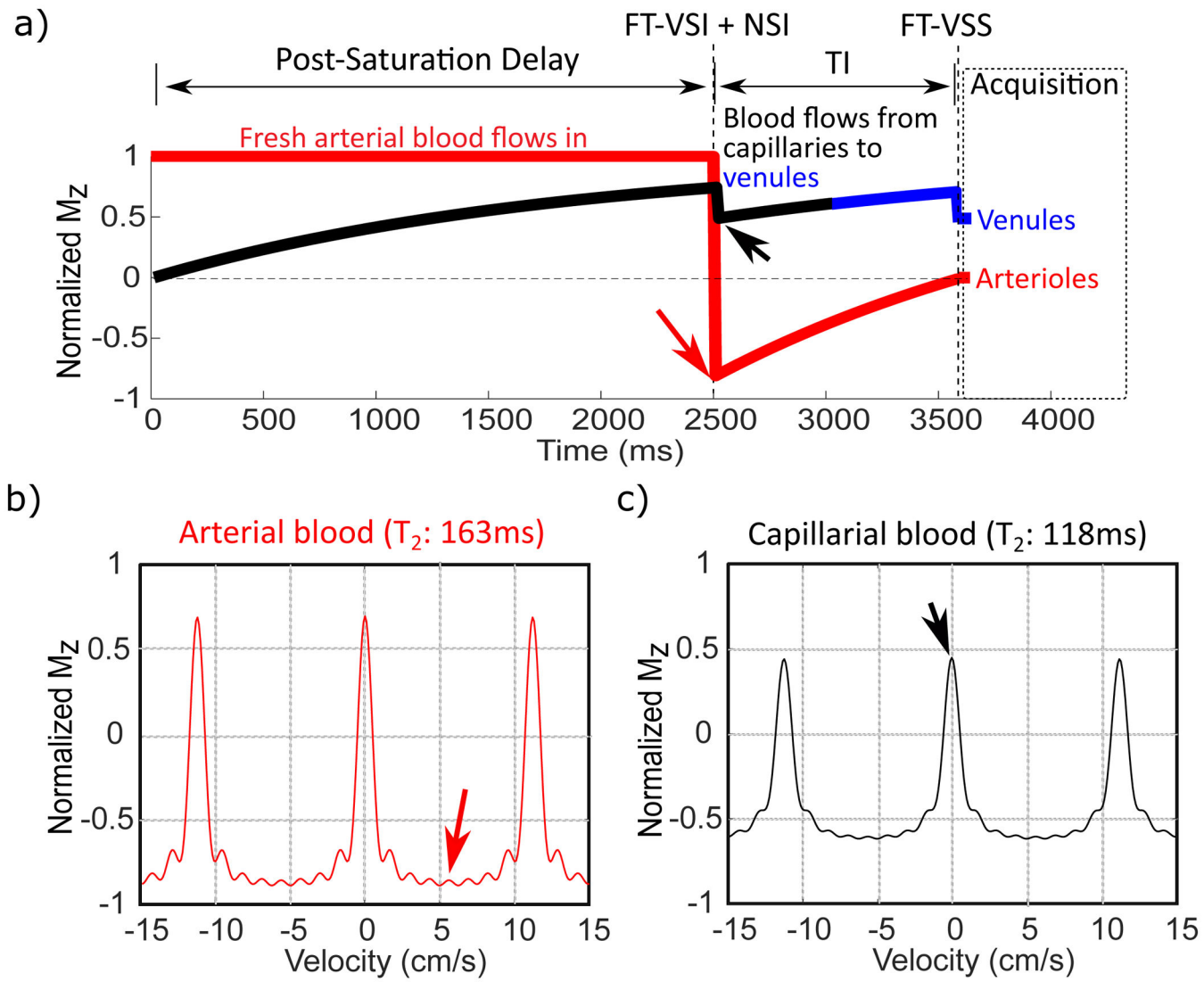

Figure 4.

a) Simulated magnetization evolution during the preparation for vCBV measurement of the spins before moving into the arterioles and venules. The arterial spins flowing above the V_{CUTOFF} would be inverted by the FT-VSI plus NSI module (efficiency 0.86, see text), then recover while flowing into the small arterioles, and finally get nulled at the end of TI (in red). The blood spins initially within the capillaries (in black) with velocity below the V_{CUTOFF} would largely flow out into the venules (in blue) during TI with the preserved signal magnetization. Meanwhile, the rest of capillary blood staying within capillary during TI is removed by the FT-VSS pulse. The Mz-velocity responses after the FT-VSI + NSI pulse trains are simulated separately by considering the T_2 relaxation effect during FT-VSI pulse trains for arterial (b) and capillary blood (c) respectively. The small signal losses right after FT-VSI + NSI and FT-VSS pulses in (a) are caused by the T_2 effect (Eq. [5] and [8]) as shown in (c).

Author Manuscript Author Manuscript Author Manuscript Author Manuscript

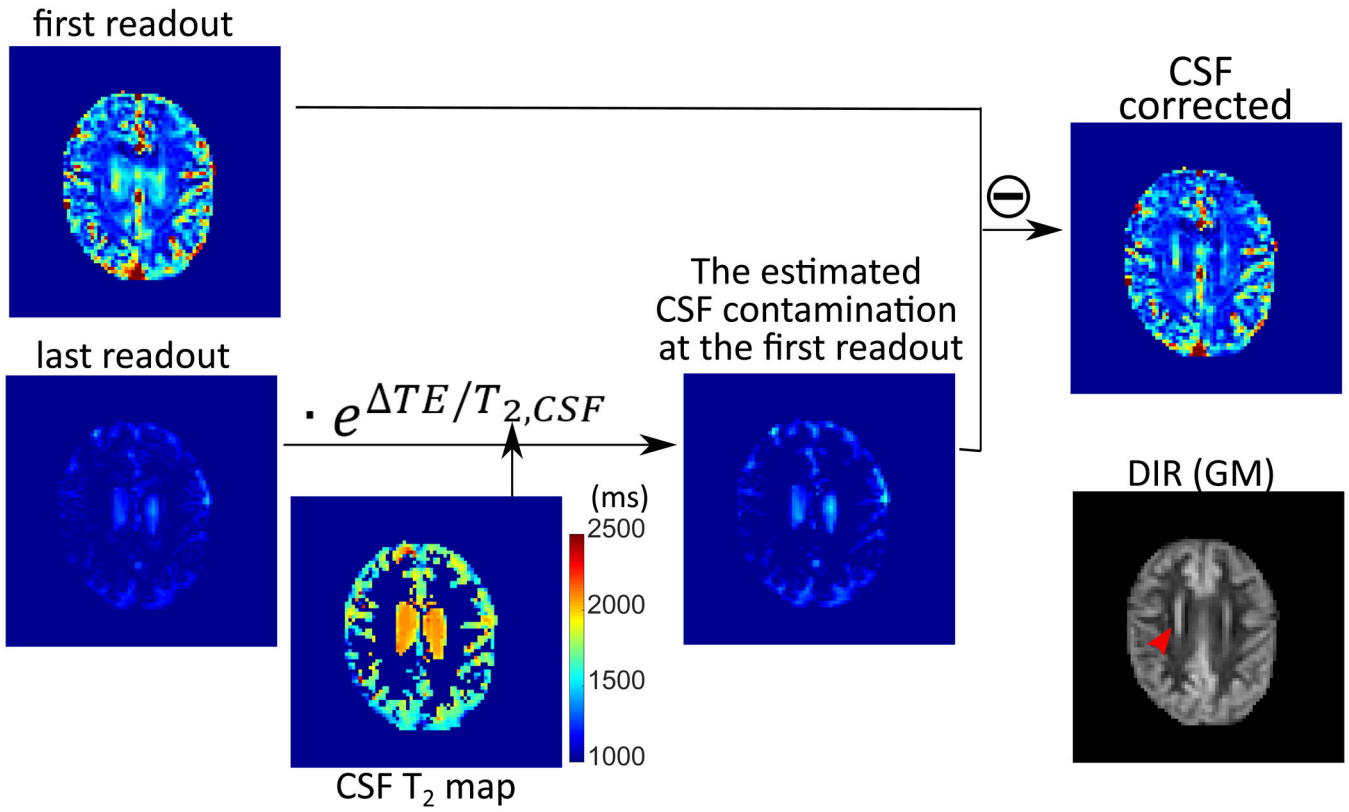

Figure 5.

Example of the process for removing CSF contamination following Eq. [2], using the label-control difference images for the CBV protocol acquired at first and last readouts . The corresponding DIR (GM) image is also shown for comparison. Note the signal of the periventricular gray matter (red arrow in DIR image), which cannot be distinguished from ventricular CSF signal in the CBV-weighted image (first readout), can be correctly represented after the CSF correction.

Author Manuscript Author Manuscript Author Manuscript Author Manuscript

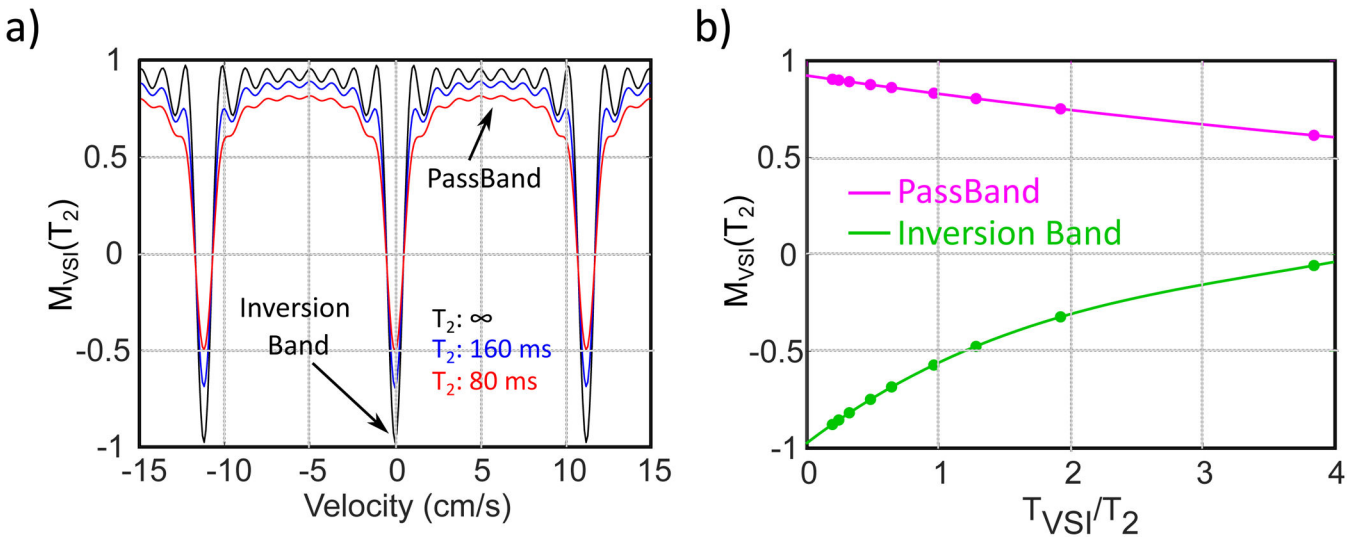

Figure 6.

a) The simulated T_2 effect on the magnetization modulation of the FT-VSI pulse train, $M_{VSI}(T_2)$, for different velocities. b) the fits of $M_{VSI}(T_2)$ for the passband (magenta) and inversion band (green) as a function of the ratio between FT-VSI pulse train length (T_{VSI}) and T_2.

Author Manuscript Author Manuscript Author Manuscript Author Manuscript

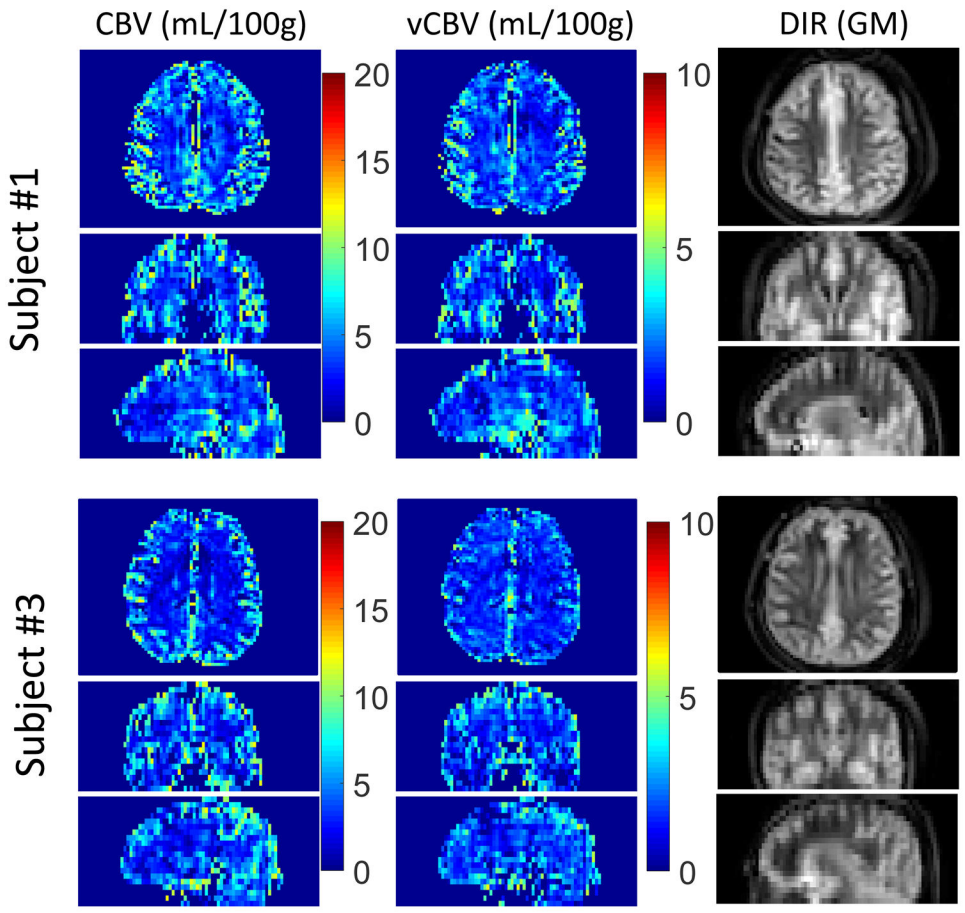

Figure 7.

Example slices from 3D maps of total CBV, vCBV and DIR (GM) for the three orthogonal planes in two subjects (#1 and #3). Note that the image scale for total CBV images is twice of that for vCBV images.

Author Manuscript Author Manuscript Author Manuscript Author Manuscript

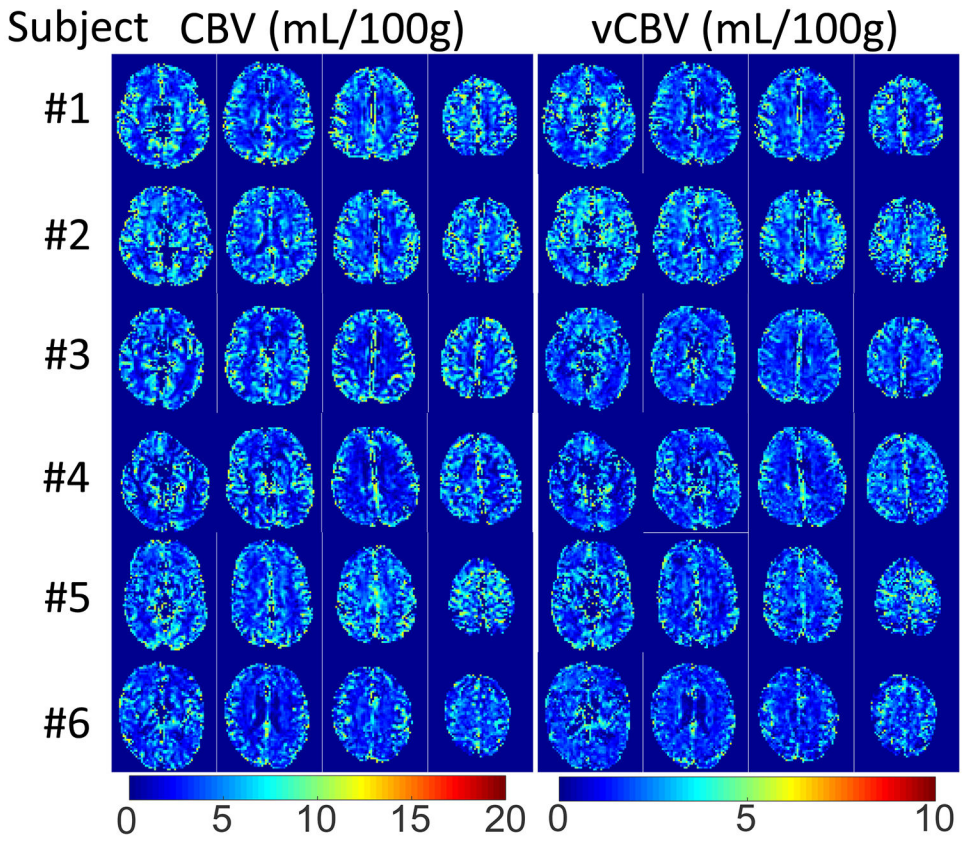

Figure 8.

Representative slices of CBV and vCBV maps acquired from all six subjects. Note that the image intensity scale for total CBV images is twice that for vCBV images.

Author Manuscript

Author Manuscript

Author Manuscript

Author Manuscript

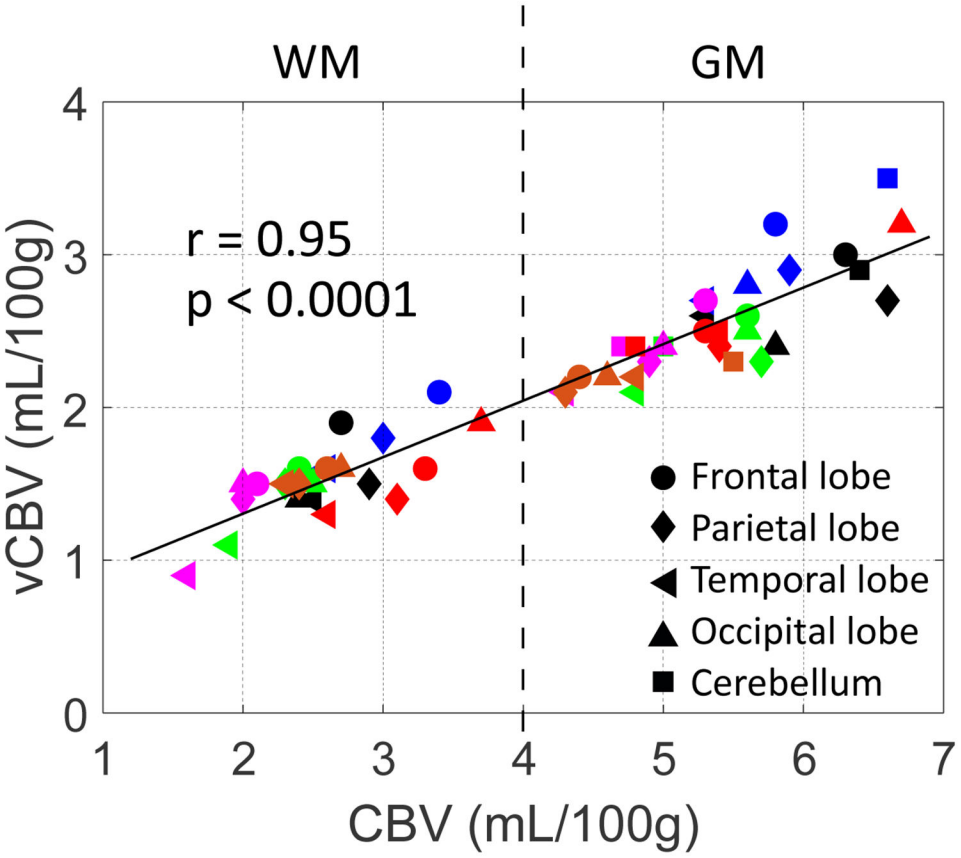

Figure 9.

Correlation of vCBV and CBV values obtained from ROIs drawn in gray matter (GM) and white matter (WM) for different cerebral regions (represented by different markers) for all our volunteers (labeled by different colors). The dashed line at CBV of 4 mL/100g separates the WM and GM ROIs. Note that in cerebellum, only GM values are reported, as WM in this area was not adequately covered with sufficient resolution.

Author Manuscript

Author Manuscript

Author Manuscript

Author Manuscript

Table 1.

Average total CBV and vCBV values in GM and WM for all six subjects.

Subject	Age (years)	CBV (mL/100g)		vCBV (mL/100g)	
		GM	WM	GM	WM
#1 (F)	38	6.0	2.8	2.8	1.5
#2(M)	35	5.8	3.0	3.0	1.9
#3 (F)	61	5.4	2.3	2.4	1.5
#4 (F)	45	4.9	1.9	2.4	1.4
#5 (F)	56	5.4	3.2	2.6	1.5
#6 (F)	61	4.5	2.3	2.1	1.4
Mean±Std	49±12	5.4±0.6	2.6±0.5	2.5±0.3	1.5±0.2